Eurasian J. For. Res. 10-1: 105-114 , 2007

Remote Sensing of Total and Surface Burn Ratios Following a Wildfire in East Siberia using 30 m–1 km Resolution Images

KUSHIDA Keiji[1]*, ISAEV Alexander P.[2], TAKAO Gen[3],
MAXIMOV Trofim C.[2] and FUKUDA Masami[1]

[1] Institute of Low Temperature Science, Hokkaido University
Sapporo 060-0819, Japan
[2] Institute for Biological Problems of Cryolithozone, Russian Academy of Science
Lenin Avenue 41, Yakutsk 677891, Russia
[3] Hokkaido Research Center, Forestry and Forest Products Research Institute
Sapporo 062-8516, Japan

Abstract

We evaluated the estimation of the area ratios of the land categories including the total-burn/wither and surface-burn areas following a wildfire in East Siberia. We obtained the land classification from 30-m resolution Landsat ETM+ image data and used it for evaluating the estimation of the area ratios of the land categories in each pixel by using 500-m and 1-km resolution images, which were generated to simulate six of the MODIS visible-to-shortwave-infrared bands. The 30-m resolution classification image was effective for the evaluation since the classification was consistent with the interpretation of the two IKONOS images obtained prior to and following the fire. The spectral mixture analysis (SMA) and multiple linear regression analysis (MLRA) were used from the viewpoints of the area ratio estimation of each land category in one pixel and in the entire study area. As a result, the 500-m resolution image provided more congruent results than the 1-km resolution image in both the SMA and MLRA. The area ratios of the total burn and surface burn were estimated using the SMA with the 500-m resolution image with 6% and 3% errors, respectively. The total-burn area and surface-burn area in the study area were estimated to be 3.8 (%) and 28.6 (%), which was an underestimation of 3% and overestimation of 38%, respectively. Although the MLRA required a wide reference image, it yielded an improved estimate of the surface-burn area. The estimation was tested in a scene immediately following the fire; this scene barely revealed the burn scars caused several years ago. Further investigation is necessary for the mapping of the total burn/wither and surface burn areas in East Siberia.

Key words: Boreal forest fire, Fire severity, Remote sensing, Spectral mixture analysis, Surface fire

1. Introduction

Wildfires in Siberian boreal forests influence the regional and global environments through the emission of aerosols (Spichtinger *et al*. 2004) and greenhouse gases into the atmosphere during combustion (Kajii *et al*. 2002), increased post-fire soil respiration (Machimura *et al*. 2005), and the changes in the thermal and hydrological conditions of the soil that occurred during vegetation recovery (Iwahana *et al*. 2005). Further, fire chronological analyses combined with the climate data for Central Siberia indicate that the fire frequency increases with the air temperature increase that is predicted for this century (Kharuk *et al*. 2005).

The burnt areas of the boreal forest and the other landscapes including mires, the tundra, post-fire areas, deforested areas, sparse forests, and grassy glades in 1988–1992 in Russia are estimated at 1.5 and 2.0 million ha/yr, respectively (Shvidenko and Nilsson, 2000), while the boreal forest area in Russia is 760 million ha (Shvidenko and Nilsson, 2002). These inventory data are based on detailed investigations carried out over a wide area; however, coupling and inter-comparison with remotely sensed data are necessary for immediately and objectively covering a wide area. The burnt areas in Russia have been estimated (Conard *et al*. 2002; Sukhinin *et al*. 2004; Soja *et al*. 2004) using the hotspot detection algorithms presented by Kaufman *et al*. (1998) or Fraser *et al*. (2000) with the thermal bands of the Advanced Very High Resolution Radiometer (AVHRR) onboard the NOAA. However, these estimates showed some disagreement with the inventory data or the Russian statistic data. For example, the Russian statistic data show a tendency to underestimate the burnt area in comparison with the average fire return intervals (larch: 90–130 years and pine: 25–50 years) (Conard and Ivanova 1997). One of the remarks on the satellite estimations concerns the spatial resolution of the remote sensors. The burnt-area ratios in one pixel of the AVHRR (1.1 km × 1.1 km) were not precisely determined using the hotspot detection algorithms. In these algorithms, a low-temperature broad fire is

(Received; Feb. 5, 2007: Accepted; March 23, 2007) ∗ Corresponding author: kkushida@lowtem.hokudai.ac.jp

confused with a high-temperature narrow fire in one pixel (Pozo *et al*. 1997). Thus, further investigations are required for fine-tuning the estimations.

With regard to the 30-m resolution sensors, White *et al*. (1996) and van Wagtendonk *et al*. (2004) used the Landsat (visible to shortwave-infrared bands) for evaluating the burnt area and the burn-severity maps in the USA mainland based on the ground-observed composite burn index (CBI). Epting *et al*. (2005) applied this method to Alaskan boreal forest fires.

In East Siberia, the evaluations of the burnt areas and their severity with a 30-m resolution (visible to shortwave-infrared bands) have barely been studied, while the boreal forest in East Siberia has characteristics identical to those of the deciduous needle-leaf larch (*Larix cajanderi* Mayr. and *Larix gmelinii* Gord.), which is the dominant species, and the surface fire that burns only the forest floor is more dominant than the crown fire (Furyaev, 1996). The evaluations with lower resolution sensors are necessary for covering continental scales without cloud contaminations. Spectral mixture analysis (SMA) has been used for estimating the area ratios of land categories in one pixel (e.g., Defries *et al*., 2000; Dennison and Roberts 2003; Rogge *et al*., 2006). In this study, we focused on the estimation of total-burn/wither and surface-burn maps after a wildfire in East Siberia using the data obtained from 30-m resolution Landsat ETM+ data; further, we have discussed the estimation of the area ratios of the two severity types using 500-m and 1-km resolution sensors.

2. Materials and Methods

2.1. Site specifications

We selected an area of 10 km × 10 km (62°15–20′N 129°30–37′E, 220 m asl) for our study; this area is located 30 km northwest of Yakutsk in the East Siberian taiga. The Landsat ETM+ image (30-m resolution) recorded on August 12, 2002 (path: 122 and row: 16) and two IKONOS images (1-m resolution) recorded on July 11, 2001 and July 31, 2002 that cover the study area were used for the analyses. The tree crowns and forest floors can be distinguished in the IKONOS images. No fresh burnt scars were distributed over the study area, as seen in the IKONOS images for July 11, 2001, while the total and surface-burnt larch forests are distributed on the study area, as seen in the IKONOS images on July 31, 2002. The two IKONOS images and an inquiry revealed that some parts of the larch forests in the study area were burnt in the period from spring to summer in 2002. We selected reference sites corresponding to each of the eight land categories found in the study area (larch (*Larix cajanderi* Mayr.), total-burnt/withered larch, surface-burnt larch, birch (*Betula papyrifera* Marsh.), and pine (*Pinus sylvestris* L.) forests, dense and sparse grasslands, and water bodies), in which we conducted a field survey for the ground truth. The total-burnt/withered larch forest corresponds to the cases in which both the tree crown and forest floor were burnt or the forest floor was burnt and the tree crown was withered from the burning of the tree roots. The surface burn corresponds to the case in which the forest floor was burnt and the tree crown was live and green. The reference sites for the larch and surface-burnt larch were located in a 170-year-old larch forest with an area of 0.5 km × 1 km (Neleger site, 62°19′N–129°31′E, 220 m asl). On this site, the larch attains heights of 20 m, constitutes more than 99% of the trees higher than 1 m and has a density of 0.2 trees/m^2. The understory is dominated by the evergreen shrub *Vaccinium vitis-idaea* L., although woody plants such as *Rosa acicularis* Lindl. and herbaceous plants such as *Limnas stelleri* Trin. occur in small portions. *Vaccinium vitis-idaea* L. reaches up to a height of 10 cm. The unvegetated portions with fallen larch leaves occupy one half of the forest floor (Kushida *et al*., 2007). The topography is flat and the soil type is silty loam. In June 2002, one half of the tree stands suffered from the surface burn. The reference site of the total-burnt/withered larch forest was located in an 80-year-old larch forest with an area of 2 km × 1 km that was burnt in the period from May to July 2002 (2002 total-burnt site, 62°17′N–129°34′E, 220 m asl). Both larch and birch were present on this site before the fire. The other reference sites were situated near the Neleger site. The forest floor of the pine site comprise vegetated parts (*Vaccinium vitis-idaea* L. and *Arctostaphylos uva-ursi* (L.) Spreng.) and nonvegetated black parts that did not recover following the last fire. *Elytrigia repens* (L.) and *Carex vesicata* Meinsh were predominant in the sparse and dense grassland sites, respectively.

2.2. Satellite image analysis

The atmospheric correction of the Landsat ETM+ image was performed using ATCOR2 for Erdas Imagine 8.7 (Leica Geosystems Corp., Heerbrugg, Switzerland) with the standard parameters (mid-latitude summer, rural, 100-km scene visibility). The Landsat image was degraded by averaging with 17 × 17 and 34 × 34 pixels, and images with 510-m and 1.02-km resolutions (hereafter referred to as 500-m-IMG and 1-km-IMG, respectively) were generated. These images were used for simulating the Moderate Resolution Imaging Spectroradiometer (MODIS) sensor onboard the Terra. Table 1 shows the wavelengths of the Landsat ETM+ and MODIS bands; here, bands 1 and 2 have 250-m resolutions, while bands 3, 4, 6, and 7 have a 500-m resolution. The spectral data on each of the seven reference sites were extracted on the 30-m resolution Landsat image and used as the training data for the maximum likelihood supervised classification on the 30-m resolution image, 500-m-IMG, and 1-km-IMG.

SMA and multiple linear regression analysis (MLRA) were tested for the estimation of the area ratios of the seven land categories in one pixel of the 500-m-IMG and 1-km-IMG. In the SMA, a linear combination of the seven land categories was assumed to generate one pixel, and the mean values of the seven land categories in the pixel were assumed to be the same as those of the training data. The area ratios of the seven categories (r_i (i = 1, 2,…, 7)) were set from 0 to 1 with intervals of 0.025 based on the following

expression:

$$\sum_{i=1}^{7} r_i = 1 \qquad (1)$$

The combination of the area ratios (r_i (i = 1, 2,…, 7)) that minimizes the equation

$$\sum_{j=1}^{6}\left(\sum_{i=1}^{7} r_i R_i(\lambda_j) - B(\lambda_j)\right)^2 \qquad (2)$$

was determined as the estimated area ratio of the land categories in the pixel. Here, R_i (i = 1, 2,…, 7) and B denote the mean reflectance values of the seven land categories and the reflectance value of a pixel on the 500-m-IMG/1-km-IMG, respectively. These are the atmospherically corrected reflectance values. Without the atmospheric correction, the assumption of the linear combination does not generally hold. λ_j (j = 1, 2,…, 6) denote the six Landsat ETM+ bands (Table 1). The water body category was removed from the analysis since its area ratio was 0.1%. We assumed that the area ratio of the water body was accounted for a priori by adding the area where the water body is distributed to the total study area.

In the MLRA, each of the area ratios of the seven land categories was calculated from the result of the classification on the 30-m resolution image and used as the explained variables, and the six Landsat ETM+ bands on the 1-km-IMG were used as potential explaining variables. The backward elimination method with a reference F value of 2.0 was used for determining the explaining variables. In order to set the summation of the area ratios at 100 (%), each of the area ratios calculated by the regression equations was divided by the summation of the area ratios.

Table 1. Wavelength bands in Landsat ETM+ and MODIS.

Landsat ETM+		MODIS	
Band	Wavelength (nm)	Band	Wavelength (nm)
1	450～520	3	459～479
2	530～610	4	545～565
3	630～690	1	620～670
4	750～900	2	841～876
5	1550～1750	6	1628～1652
7	2090～2350	7	2105～2155

3. Results

3.1. Land classification using 30-m resolution image

The spectral characteristics of the training data characterize the separations into categories. Fig. 1 shows the spectral characteristics of the land categories at the eight reference sites obtained from the Landsat imagery. The standard deviations of the spectrum of each of the land categories were less than 1.6 (%) for the bands, except for the 3.2 (%) deviation in band 4. Due to the small standard deviations of the spectrums, each of these eight categories was spectrally separated from the others despite the small number of bands. The total-burnt/withered area and the surface-burnt area have higher reflectance factors in band 7 than in the forests; this tendency is reported as a characteristic of burn scars in previous studies (e.g., White *et al*., 1996). Grasslands (sparse and dense categories) also show high reflectances in band 7, although their spectral characteristics in other bands were different from those in other categories.

Fig. 2(a) shows the Landsat ETM+ imagery of the study area, and Fig. 2(b) shows the results of the maximum likelihood classification using the 30-m resolution image with the training data for the eight reference sites. A comparison of the two IKONOS images before and after the fire in the study area reveals that the land categories of the total burn/wither, surface burn, larch, birch, and pine, and the water body category were classified correctly. However, the separation between the sparse and dense grasslands was ambiguous and the boundaries of two or more categories were misclassified. The ratio of the boundary misclassification was quite small since the mean patch size of the land categories was larger in comparison to the resolution (30 m) (Fig. 2(a)). This shows that the classification using the 30-m resolution image is useful for the evaluation of the area ratio using the 500-m-IMG and 1-km-IMG.

3.2. Estimation of area ratios of land categories using 500-m and 1-km resolution images

In the 500-m-IMG and 1-km-IMG, many pixels were composed of two or more different categories; these were termed mixed pixels (mixels). Figs. 2 (c) and (d) show the result of the maximum likelihood classification using the 500-m-IMG and 1-km-IMG, respectively. The total-burnt/withered area in the middle of the image decreased, while the larch on the lower right-hand side of the image increased; this resulted from the spectral characteristics of the categories that contain the mixels. Table 2 shows the area ratios of the land categories in the study area that were obtained by the maximum likelihood classification for the three images with different resolutions. The area ratios of the categories that occupy less than 10% of the study area as estimated by using the images that simulate the MODIS were lower than those obtained from the classification using the 30-m resolution image. When the two images that simulate the MODIS were used, the total burn/wither and surface burn were underestimated by 67–75% and 10–20%, respectively, using the two images that

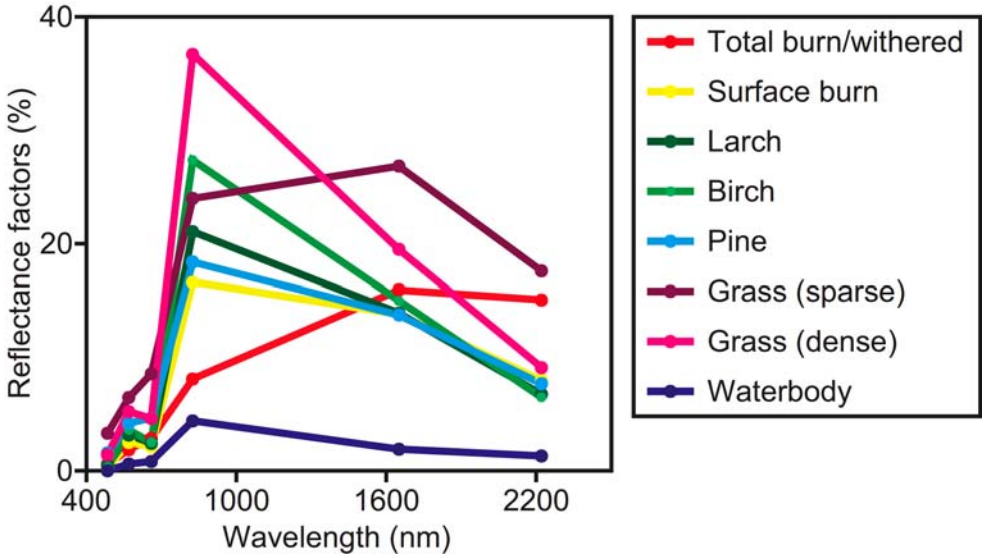

Fig. 1. Spectral characteristics of the land categories at the eight reference sites obtained from the Landsat ETM+ image 122-16 on August 12, 2002.

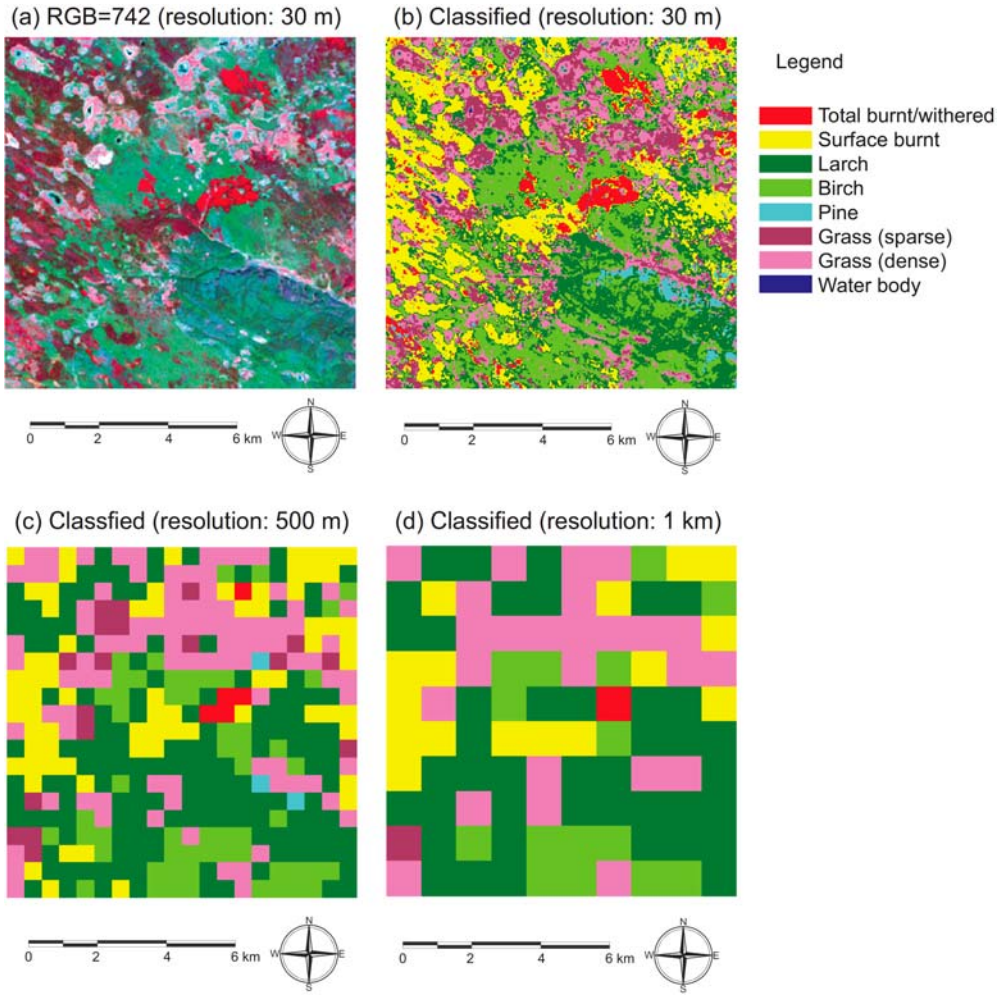

Fig. 2. (a) Landsat ETM+ image 122-16 on Aug 12, 2002 (62°15–20′N 129°30–37′E, RGB = 742, resolution: 30 m); (b) land classification using image (a) (resolution: 30 m); (c) land classification using the averaged image (a) in an area of 510 m × 510 m (resolution: 510 m); (d) land classification using the averaged image (a) in an area of 1.02 km × 1.02 km (resolution: 1.02 km).

simulate the MODIS, while the larch was overestimated by 90–110%.

The area ratios of the land categories in the mixels were estimated by SMA. Figs. 3 and 4 show the relationships between the area ratios estimated by the SMA of the 500-m-IMG and 1-km-IMG (estimated) and the 30-m resolution classification (observed) for the seven land categories, respectively. Here, the coefficient of variation (c.v.) was defined as

$$\text{c.v.} = \frac{\sqrt{\sum (r_{obs} - r_{est})^2}}{\sum r_{est}}, \qquad (3)$$

where r_{obs} and r_{est} denote the observed and estimated area ratios of each pixel. The estimation using the 500-m-IMG yielded a smaller c.v. than that using the 1-km-IMG for each of the land categories. The area ratios of grass (dense) in most of the pixels were estimated at 0–15%, which were smaller than those obtained by the observations (Figs. 3(g) and 4(g)). A probable reason for this is that the spectra of the birch and grass (dense) showed similar shapes, although the reflectance values were different (Fig. 1) and the two categories exhibited multicollinearity. Fig. 5 shows the relationships between the estimated and observed values of the total area ratios of the birch and grass (dense) categories. The total area ratio was estimated with a c.v. of 3–5%. Table 3 shows the area ratios in the study area obtained by the SMA. SMA for one 10 km × 10 km pixel representing the total study area did not provide more accurate result than that for 500-m-IMG or 1-km-IMG. For the 500-m-IMG, the total burn/wither and the total area of the birch and grass (dense) were underestimated by 3% and 19%,

Table 2. Area ratios (%) of the land categories obtained by maximum likelihood classification.

	Resolution		
	30 m	500 m	1 km
Total burn/wither	3.9	1.3	1.0
Surface burn	20.8	18.0	16.0
Larch	20.2	38.3	42.0
Birch	20.7	14.0	15.0
Pine	2.1	0.8	0.0
Grass (sparse)	7.1	4.5	1.0
Grass (dense)	25.2	23.3	25.0
Water body	0.1	0.0	0.0

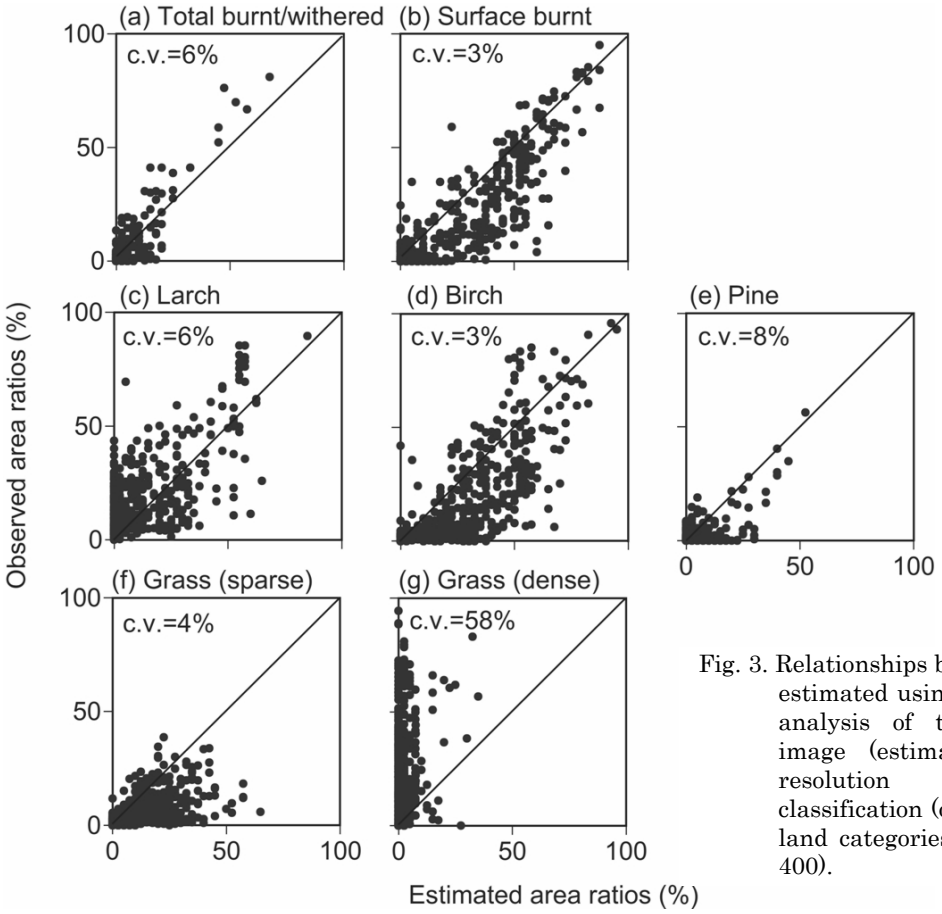

Fig. 3. Relationships between the area ratios estimated using the spectral mixture analysis of the 510-m resolution image (estimated) and the 30-m resolution Landsat ETM+ classification (observed) for the seven land categories (number of samples: 400).

respectively, while surface burn and larch was overestimated by 38% and 25%, respectively.

Figs. 6 and 7 show the relationships between the area ratios estimated by the MLRA of the 500-m-IMG and 1-km-IMG (estimated) and the 30-m resolution classification (observed), respectively. The estimation using the 500-m-IMG provided a lesser c.v. than that using the 1-km-IMG for each of the land categories, although the regression equations were obtained using the 1-km-IMG. In the total burn/wither and pine, the estimation by the MLRA yielded a higher c.v. than that by the SMA. In other land categories, the estimation by the MLRA yielded a lower c.v. than that by the SMA. The calculated total area ratios of one pixel showed a

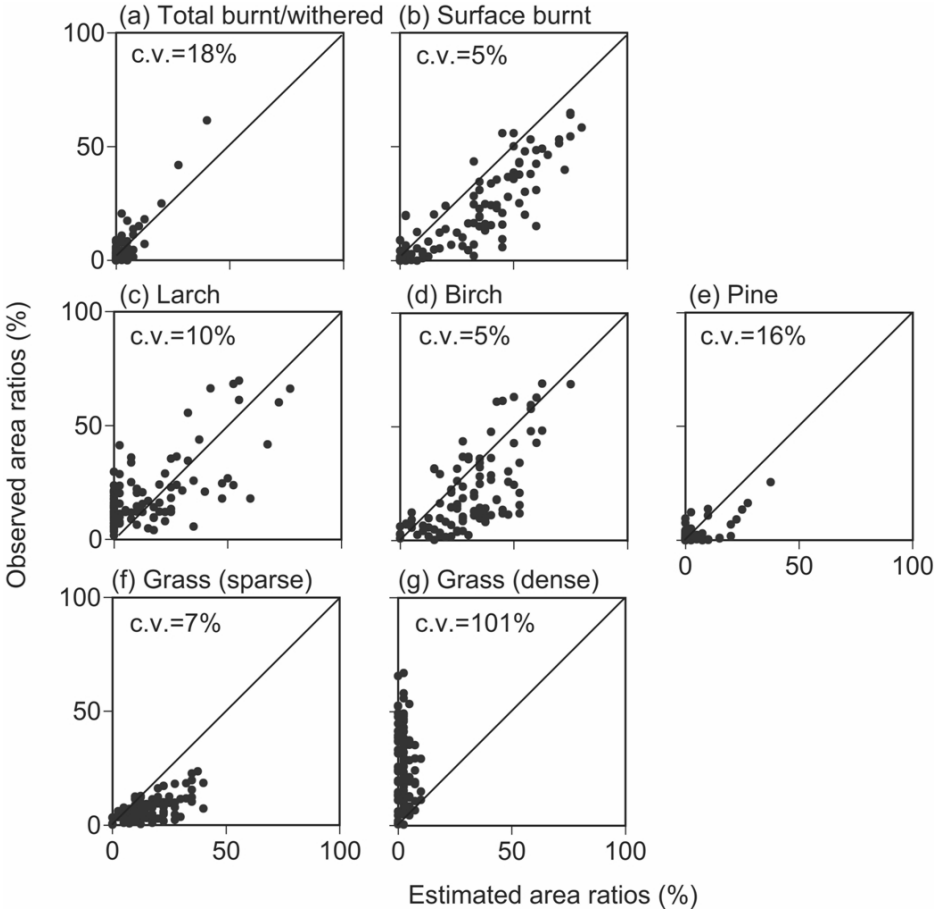

Fig. 4. Relationships between the area ratios estimated using the spectral mixture analysis of the 1.02-km resolution image (estimated) and the 30-m resolution Landsat ETM+ classification (observed) for the seven land categories (number of samples: 100).

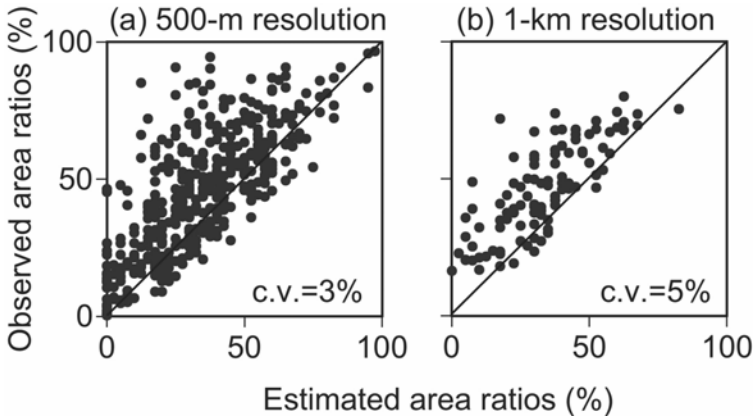

Fig. 5. Relationships between the total area ratios of the birch and grass (dense) categories estimated using the spectral mixture analysis of the (a) 510-m and (b) 1.02-km resolution images (estimated) and the 30-m resolution Landsat ETM+ classification (observed).

distribution in the range of 89–141 (%) (the minimum and maximum values) with an average of 104 (%). Further, a standard deviation of 7 (%) was obtained for the 500-m-IMG, and a distribution over 92–114 (%) (the minimum and maximum values) with an average of 101 (%) and a standard deviation of 3 (%) was obtained for the 1-km-IMG. Table 4 shows the area ratios in the study area obtained using the MLRA. Each of the estimated area ratios of the land categories in the study area was almost similar to the observed value obtained by using the MLRA, except for the total burn/wither, which was overestimated by 23–31%. Table 5 shows the regression equations for estimating the area ratios of the land categories. The area ratio of the total burn/wither was estimated with three near-infrared to shortwave-infrared bands, and that of the surface burn was estimated with three near-infrared to shortwave-infrared bands and the red band.

Table 3. Area ratios (%) of the land categories obtained by spectral mixture analysis.

	Observation	Spectral mixture analysis		
	30 m	500 m	1 km	10 km
Total burn/wither	3.9	3.8	2.5	0
Surface burn	20.8	28.6	31.2	35.0
Larch	20.2	14.0	15.1	15.0
Birch	20.7	31.9	30.0	32.5
Pine	2.1	4.0	3.0	0
Grass (sparse)	7.1	15.1	15.5	17.5
Grass (dense)	25.2	2.7	2.8	0
Water body	0.1	-	-	-

Table 4. Area ratios (%) of the land categories obtained by multiple linear regression analysis.

	Observation	multiple linear regression analysis	
	30 m	500 m	1 km
Total burn/wither	3.9	5.1	4.8
Surface burn	20.8	21.9	21.1
Larch	20.2	20.0	19.8
Birch	20.7	21.8	21.0
Pine	2.1	2.5	2.3
Grass (sparse)	7.1	7.1	7.0
Grass (dense)	25.2	25.5	25.3
Water body	0.1	-	-

Table 5. Regression equations for estimating the area ratios (%) of the land categories.

	Regression equations						R^2
Total burn/wither				$6.11B4$	$-21.9B5$	$+26.7B7$	-8.2	0.69
Surface burn			$-21.2B3$	$-12.0B4$	$+27.0B5$	$-20.0B7$	$+90.4$	0.60
Larch		$-14.0B2$	$+32.2B3$	$-3.47B4$		$-20.3B7$	$+221.9$	0.69
Birch	$-22.8B1$			$+16.8B4$	$-31.8B5$	$+32.2B7$	-97.8	0.87
Pine	$10.4B1$		$+4.62B3$	$-1.82B4$		$-4.86B7$	$+62.5$	0.45
Grass (sparse)	$21.7B1$	$-9.46B2$		$+1.50B4$			-7.2	0.62
Grass (dense)		$9.62B2$	$-10.6B3$	$-6.28B4$	$+26.3B5$	$-14.7B7$	-137.2	0.87

B1, *B2*, *B3*, *B4*, *B5*, and *B7* denote Landsat ETM+ bands 1, 2, 3, 4, 5, and 7, respectively.

4. Discussions

We obtained the land classification including the total burn/wither and surface burn area following a wildfire in East Siberia from 30-m resolution Landsat ETM+ data and used it to evaluate the estimation of the area ratios of the land categories in each pixel by the SMA and MLRA using the 500-m-IMG and 1-km-IMG. The 30-m resolution classification image was effective for the evaluation since the classification was consistent with the interpretation of the two IKONOS images before and after the fire.

We observed that the use of the 500-m-IMG, in comparison to the use of the 1-km-IMG, yielded SMA and MLRA results that were in greater agreement from the viewpoints of the c.v. value of the area ratio estimate for each land category in one pixel and in the entire study area. Finer resolution images are important for overlaying information such as the biomass and carbon budget structures before the fire. Kushida *et al*. (2007) showed that the leaf-area index and forest-floor vegetation cover are the indicators of the net primary productivity of larch in East Siberia and estimated the geographical distribution of these indicators using the Landsat ETM+ data. The combination of this information with the knowledge of the fire severity (total burn/wither or surface burn) could facilitate the further evaluation of the fire and its influence on the environmental changes.

The average spectra of the land categories are required for the application of the SMA to the MODIS data, while images such as the Landsat ETM+ data are required for the MLRA. In the total burn/wither and pine areas, the estimation by the SMA yielded a lower c.v. than that by the MLRA; in the other land categories, however, the estimation by the MLRA yielded a lower c.v. than that by the SMA. One of the reasons for the overestimation and underestimation of the area ratios in the SMA was due to the discord between the reference and real spectra of the land categories. In the MLRA, the average spectrum of the land categories in the reference and the real data are equalized. However, in the MLRA, the total area ratio of one pixel has to be adjusted after the calculation of the area ratios of the land categories. This can lead to a higher c.v. in the total burn/wither and pine areas obtained in the MLRA, as compared to that obtained in the SMA. In the SMA using the 500-m-IMG, the total-burnt area and the surface-burnt area were estimated as 3.8 (%) and 20.8 (%), respectively, in the study area; the corresponding values of these areas obtained by using the 30-m resolution image were 3.9 (%) and 28.6 (%), respectively.

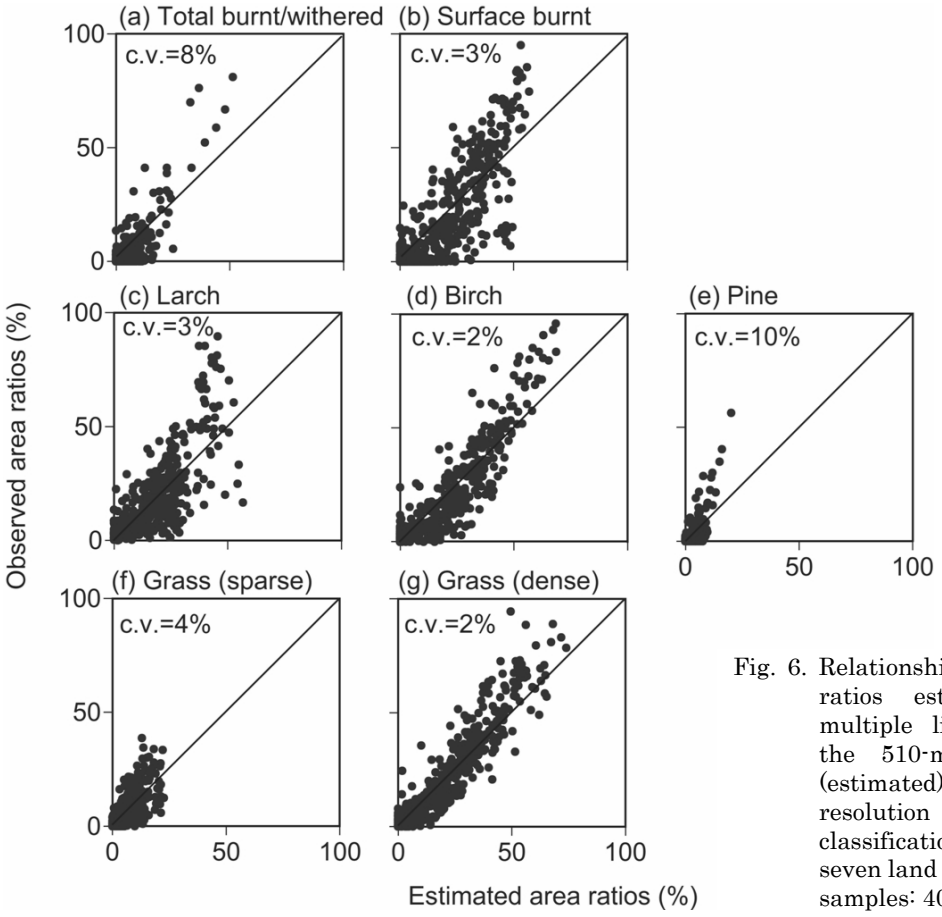

Fig. 6. Relationships between the area ratios estimated using the multiple linear regressions of the 510-m resolution image (estimated) and the 30-m resolution Landsat ETM+ classification (observed) for the seven land categories (number of samples: 400).

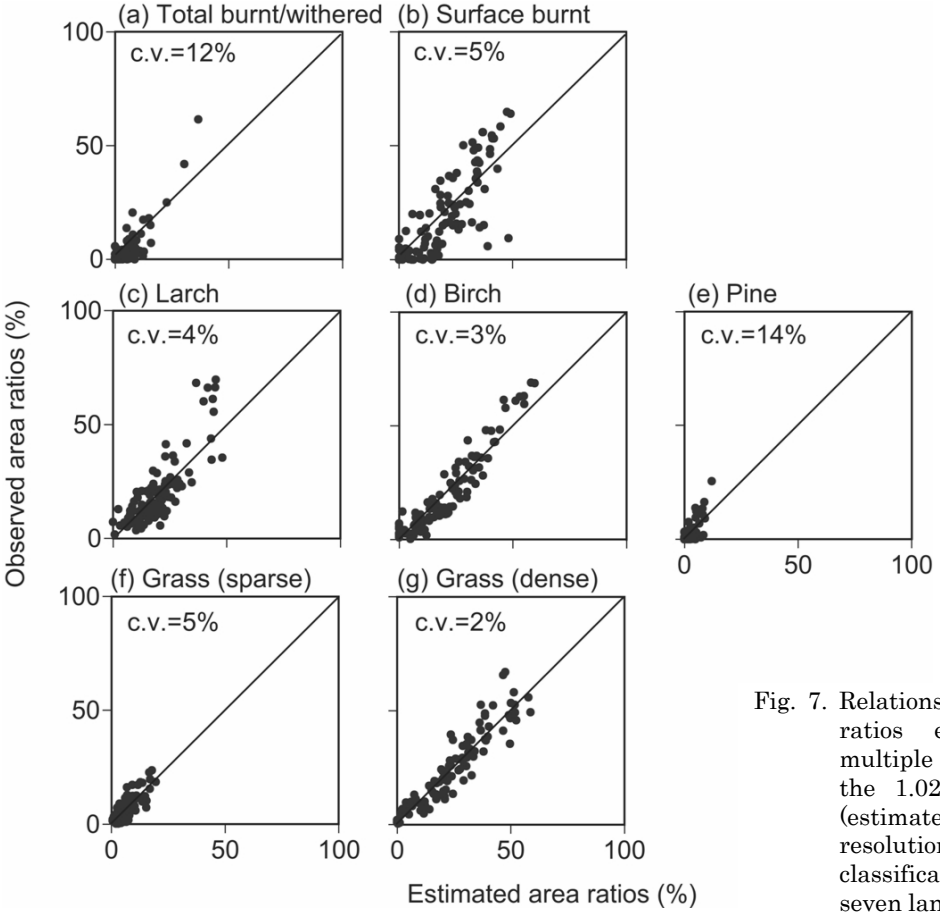

Fig. 7. Relationships between the area ratios estimated using the multiple linear regressions of the 1.02-km resolution image (estimated) and the 30-m resolution Landsat ETM+ classification (observed) for the seven land categories (number of samples: 100).

The band choices obtained for estimating the total burn/wither by the MLRA were consistent with those reported by George *et al*. (2006); this consistency indicates the effectiveness of the indices of the near-infrared to shortwave-infrared bands for extracting the burnt areas in Siberia. In the area ratio estimations of the seven land categories by the MLRA, band 4 was used for all the seven categories and band 7 was used for six out of the seven categories. These two bands—4 and 7—were used for estimating the composite burn index (e.g., Epting *et al*., 2005).

5. Conclusion

In this study, we evaluated the estimation of the area ratios of the land categories including the total burnt/withered and surface-burnt areas after a wildfire in East Siberia by SMA and MLRA using 500-m and 1-km resolution images; these analyses simulate six MODIS visible to shortwave-infrared bands. The 500-m resolution image yielded more congruent results than the 1-km resolution image in both the SMA and the MLRA from the viewpoints of the area ratio estimation of each land category in one pixel and in the entire study area. The area ratios of the total-burnt and surface-burnt areas were estimated using the SMA with the 500-m resolution image with 6% and 3% errors, respectively. The SMA using the 500-m resolution image yielded an estimate of the total burnt area of 3.8 (%) and surface burnt area of 28.6 (%) in the study area, which was an underestimation of 3% and overestimation of 38%, respectively. The estimation of the surface-burnt area was improved by using the MLRA, although a wide reference image was required. The burnt-area mapping with the SMA and MLRA may contribute to evaluating the emission of aerosols and greenhouse gases into the atmosphere during combustion, post-fire soil respiration, and vegetation recovery. In this study, we focused on the estimation in a scene immediately following the fire and the scene barely revealed burn scars caused several years ago. Further investigations are necessary for the mapping of the total-burnt/withered and surface-burnt areas in East Siberia.

Acknowledgements

The authors wish to thank Takayoshi KOIKE, Ryusuke HATANO, Minoru TERAZAWA, Fuyuki SATOH of Hokkaido University, and two anonymous reviewers for their helpful suggestions. This study was supported by the Global Environment Research Fund (B-053) of the Japan Ministry of Environment, the Research Revolution 2002 (RR2002) program of the Japan Ministry of Education, Culture, Sports, Science and Technology (MEXT), and the Core to Core Program of the Japan Society for the Promotion of Science (JSPS).

References

Conard, S.G. and Ivanova, G.A. (1997) Wildfire in Russian boreal forests - Potential impacts of fire regime characteristics on emissions and global carbon balance estimates. Environ. Pollut., 98: 305-313.

Conard, S.G., Sukhinin, A.I., Stocks, B.J., Cahoon, D.R., Davidenko, E.P. and Ivanova, G.A. (2002) Determining effects of area burned and fire severity on carbon cycling and emissions in Siberia. Climate Change 55: 197-211.

Defries, R.S., Hansen, M.C. and Townshend, J.R.G. (2000) Global continuous fields of vegetation characteristics: a linear mixture model applied to multi-year 8 km AVHRR data. Int. J. Remote Sens., 21: 1389-1414.

Dennison, P.E. and Roberts, D.A. (2003) Endmember selection for multiple endmember spectral mixture analysis using endmember average RMSE. Remote Sens. Environ., 87: 123-135.

Epting, J., Verbyla, D. and Sorbel, B. (2005) Evaluation of remotely sensed indices for assessing burn severity in interior Alaska using Landsat TM and ETM+. Remote Sens. Environ., 96: 328-339.

Fraser, R.H., Li, Z. and Cihlar, J. (2000) Hotspot and NDVI differencing synergy (HANDS): A new technique for burned area mapping over boreal forest. Remote Sens. Environ., 74: 362-376.

Furyaev, V.V. (1996), Pyrological regimes and dynamics of the southern taiga forests in Siberia. In: Goldammer, J.G. and Furyaev, V.V. (eds.) Fire in ecosystems of boreal Eurasia. Kluwer Academic Publishers Dordrecht, the Netherlands, 168-185.

George, C., Rowland, C., Gerard, F. and Balzter, H. (2006) Retrospective mapping of burnt areas in Central Siberia using a modification of the normalized difference water index. Remote Sens. Environ., 104: 346-359.

Iwahana, G., Machimura, T., Kobayashi, Y., Fedorov, A.N., Konstantinov, P.Y. and Fukuda, M. (2005) Influence of forest clear-cutting on the thermal and hydrological regime of the active layer near Yakutsk, eastern Siberia. J. Geophys. Res., 110(G02004): doi:10.1029/2005JG000039.

Kajii, Y., Kato, S., Streets, D.G., Tsai, N.Y., Shvidenko, A., Nilsson, S., McCallum, I., Minko, N.P., Abushenko, N., Altyntsev, D. and Khodzer, T.V. (2002) Boreal forest fires in Siberia in 1998: Estimation of area burned and emissions of pollutants by advanced very high resolution radiometer satellite data. J. Geophys. Res., 107(D24): 4745, doi:4710.1029/2001JD001078.

Kaufman, Y.J., Justice, C.O., Flynn, L.P., Kendall, J.D., Prins, E.M., Giglio, L., Ward, D.E., Menzel, W.P. and Setzer, A.W. (1998) Potential global fire monitoring from EOS-MODIS. J. Geophys. Res., 103(D24): 32215-32238.

Kharuk, V.I., Dvinskaya, M.L. and Ranson, K.J. (2005) The spatiotemporal pattern of fires in northern Taiga larch forests of central Siberia. Russian J. Ecol., 36: 302-311.

Kushida, K., Isaev, A.P., Maximov, T.C., Takao, G., and Fukuda, M. (2007) Remote sensing of upper canopy leaf area index and forest floor vegetation cover as indicators of net primary productivity in a Siberian larch forest. J. Geophys. Res., doi:10.1029/2006JG000269, in press.

Machimura, T., Kobayashi, Y., Iwahana, G., Hirano, T., Lopez, L., Fukuda, M. and Fedorov, A.N. (2005) Change of carbon dioxide budget during three years after deforestation in eastern Siberian larch forest. J. Agric. Meteorol., 60: 653-656.

Pozo, D., Olmo, F.J. and AladosArboledas, L. (1997) Fire detection and growth monitoring using a multitemporal technique on AVHRR mid-infrared and thermal channels. Remote Sens. Environ., 60: 111-120.

Rogge, D.M., Rivard, B., Zhang, J. and Feng, J. (2006) Iterative spectral unmixing for optimizing per-pixel endmember sets. IEEE Trans. Geosci. Remote Sens., 44: 3725-3736.

Shvidenko, A., and Nilsson, S. (2000) Extent, distribution, and ecological role of fire in Russian forests. *In:* Kasischke, E.S., and Stocks, B.J. (eds.) Fire, climate change, and carbon cycling in the boreal forest. Springer-Verlag, New York, USA, 132-150.

Shvidenko, A., and Nilsson, S. (2002) Dynamics of Russian forests and the carbon budget in 1961-1998: An assessment based on long-term forest inventory data. Clim. Change, 55: 5-37.

Soja, A.J., Sukhinin, A.I., Cahoon, D.R., Shugart, H.H. and Stackhouse, P.W. (2004) AVHRR-derived fire frequency, distribution and area burned in Siberia. Int. J. Remote Sens., 25: 1939-1960.

Spichtinger, N., Damoah, R., Eckhardt, S., Forster, C., James, P., Beirle, S., Marbach, T., Wagner, T., Novelli, P.C. and Stohl, A. (2004) Boreal forest fires in 1997 and 1998: a seasonal comparison using transport model simulations and measurement data. Atmos. Chem. Phys., 4: 1857-1868.

Sukhinin, A.I., French, N.H.F., Kasischke, E.S., Hewson, J.H., Soja, A.J., Csiszar, I.A., Hyer, E.J., Loboda, T., Conrad, S.G., Romasko, V.I., Pavlichenko, E.A., Miskiv, S.I. and Slinkina, O.A. (2004) AVHRR-based mapping of fires in Russia: New products for fire management and carbon cycle studies. Remote Sens. Environ., 93: 546-564.

van Wagtendonk, J.W., Root, R.R. and Key, C.H. (2004) Comparison of AVIRIS and Landsat ETM+ detection capabilities for burn severity. Remote Sens. Environ., 92: 397-408.

White, J.D., Ryan, K.C., Key, C.C. and Running, S.W. (1996) Remote sensing of forest fire severity and vegetation recovery. Int. J. Wildland Fire, 6: 125-136.